RESEARCH ARTICLE

Emergent Protective Organogenesis in Date Palms: A Morpho-devo-dynamic Adaptive Strategy During Early Development.

Ting Ting Xiao[1], Alejandro Aragón Raygoza[2], Juan Caballero Pérez[2], Gwendolyn Kirschner[1], Yanming Deng[3], Brian Atkinson[4], Craig Sturrock[4], Vinicius Lube[5] Jian You Wang[1], Gilles Lubineau[5], Salim al Babili[1], Alfredo Cruz Ramírez[2], Malcolm Bennett[4] and Ikram Blilou[1*]

Affiliations

[1]King Abdullah University of Science and Technology (KAUST), Biological and Environmental Sciences and Engineering (BESE), Thuwal, 23955-6900, Saudi Arabia

[2]Molecular and Developmental Complexity Group, Unidad de Genómica Avanzada-Laboratorio Nacional de Genómica para la Biodiversidad (LANGEBIO), CINVESTAV, Irapuato, Guanajuato, México

[3]Provincial Key Laboratory for Horticultural Crop Genetic Improvement, Institute of Leisure Agriculture, Jiangsu Academy of Agricultural Sciences, Nanjing, Jiangsu, China

[4]Hounsfield Facility, School of Biosciences, University of Nottingham, Nottingham, LE12 3RD, UK

[5]King Abdullah University of Science and Technology (KAUST), Physical Science and Engineering Division, COHMAS Laboratory, Thuwal 23955-6900, Saudi Arabia

*Corresponding author

Short Title: Morpho-devo-dynamics in date palms

One-sentence summary: Date palm uses unique developmental modes to protect its embryo and organs by pausing development during germination and confining developing organs within a multilayered structure in early development

The author responsible for distribution of materials integral to the findings presented in this article in accordance with the policy described in the Instructions for Authors (www.plantcell.org) is: Ikram Blilou (ikram.blilou@kaust.edu.sa).

ABSTRACT

Desert plants have developed mechanisms for adapting to hostile desert conditions, yet these mechanisms remain poorly understood. Here, we describe two unique modes used by desert date palms (*Phoenix dactylifera* L.) to protect their meristematic tissues during early organogenesis. We used X-ray micro-computed tomography combined with high-resolution tissue imaging to reveal that, after germination, development of the embryo pauses while it remains inside a dividing and growing cotyledonary petiole. Transcriptomic and hormone analyses show that this developmental arrest is associated with the low expression of development-related genes and accumulation of hormones that promote dormancy and confer resistance to stress. Furthermore, organ-specific cell type mapping demonstrates that organogenesis occurs inside the cotyledonary

petiole, with identifiable root and shoot meristems and their respective stem cells. The plant body emerges from the surrounding tissues with developed leaves and a complex root system that maximizes efficient nutrient and water uptake. We further show that, similar to its role in *Arabidopsis thaliana*, the SHORT-ROOT (SHR) homologue from date palms functions in maintaining stem cell activity and promoting formative divisions in the root ground tissue. Our findings provide insight into developmental programs that confer adaptive advantages in desert plants that thrive in hostile habitats.

INTRODUCTION

The process through which a complex adult form emerges from a cascade of developmental events, tightly controlled in space and time, is called morphogenesis. Changes in environmental conditions can modulate this process, thus providing an adaptive developmental plasticity to overcome environmental challenges. In animals, diapause causes a temporary arrest in development to allow the embryo to survive harsh conditions and to ensure that postnatal development can be completed when environmental conditions become more favorable (Apfeld and Kenyon, 1998; Fenelon et al., 2014; Liu et al., 2016; Fielenbach and Antebi, 2008). In plants, this process is called dormancy during which a fully developed embryo rests inside the seed. Under optimal conditions, the seed germinates and produces a seedling that grows and continuously generates organs that form the adult plant body. Dormancy and diapause are primarily linked to survival in low temperatures during winter. However, high-temperature-induced diapause or dormancy has been observed in worms, insects and plants (Wadsworth et al., 2013).

The date palm (*Phoenix dactylifera* L.) is one of the few fruit trees that, remarkably, can grow in the desert, a habitat with an arid climate where extreme temperature changes and drought conditions limit plant growth. Date fruits are essential for sustaining current desert agriculture production. However, breeding strategies aimed at improving date palm production are hindered by the long generation time (fruit production starts 5 to 10 years after planting) and their dioecious nature (male and female flowers on different trees), in addition to the large phenotypic variation in progeny caused by heterozygosity (El Hadrami, et al., 2011).

To cope with changes in their surrounding environment, palms have adopted three morphologically distinct modes of germination (Pinheiro, 2001; Baskin and Baskin, 2014)

(Supplementary Figure 1A): 1) adjacent ligular: the cotyledon sheath with the embryo is located directly next to the seed; 2) remote ligular: the cotyledon extends to form a petiole connecting the haustorium to the cotyledon ligule; 3) remote tubular: a petiole forms and becomes a tubular structure instead of a ligule (Demason, 1988b, 1984; Iossi et al., 2006; Tillich, 2007; Henderson, 2006). Date palms germinate by the remote tubular mode; germination begins in this case with the emergence of a root-like structure termed the cotyledonary petiole. This structure elongates to form the primary root and a plumule that, together with the primary leaf, emerge through an opening/cleavage from the cotyledonary petiole (Demason, 1988b, 1984; Iossi et al., 2006; Tillich, 2007).

Later in development, the date palm develops an intricate root system that comprises the main root and the anchor roots that grow vertically, secondary roots that grow laterally, and negatively geotropic roots that grow above-ground (called pneumatophores) (Jost, 1887; Granville, 1974; Seubert, 1997). A root often supports multiple pneumatophores, forming the pneumatorhiza (Seubert, 1997; Dreyer et al., 2010). In date palms, the primary root consists of multiple tissue types: the outermost layers form the rhizodermis/velamen (r/v) that surrounds the exodermis, which in turn surrounds two types of cortex tissues, and the outer cortex (oc) and the inner cortex (ic). Inside the ic, where intercellular spaces form the aerenchyma, lies the endodermis that surrounds the vascular cylinder (vc) (Granville, 1974; Drabble, 1903; Seubert, 1997).

A detailed characterization of early developmental programs in date palms and study of its adaptation to arid conditions is currently lacking, despite the available body of literature on date palm anatomy and growth (Iossi et al., 2006; Seubert, 1997; Henderson, 2006; Pinheiro, 2001; Drabble, 1903; Fls, 2006; Seubert, 1996) and the extensive efforts made on date palm genomics, proteomics and metabolomics (Al-dous et al., 2011; Hazzouri et al., 2015; Al-Mssallem et al., 2013; Stephan et al., 2018; Marondedze et al., 2014). Addressing these knowledge gaps could provide important foundational knowledge for the expansion of desert agriculture production, which will be essential in the face of global climate change.

Here we present a comprehensive study of the early development of date palms, from germination to seedling stage. Germination in date palms begins with the emergence of the cotyledonary petiole. We found that the undeveloped embryo resides within the growing tip of the cotyledonary petiole. This developmental embryonic pause coincides with a reduced rate of

cell division, reduced expression of key developmental genes and an accumulation of hormones associated with dormancy, as well as with responses to abiotic and biotic stresses. Remarkably, we observed that organogenesis occurs within the cotyledonary petiole. The developing seedling remains encapsulated and produces root, shoot and leaf primordia that express organ specific genes. As growth continues, the leaf protrudes through the surrounding tissue. The shoot meristem produces new primordia that proliferate and elongate, which in turn allow the date palm above-ground organs to increase in diameter and height.

We found that as the plant grows, the cotyledonary petiole tip/radicle elongates giving rise to the future root. This is in contrast to grasses where the root, before penetrating the soil, splits from the coleorhiza, a non-vascularized multicellular embryonic tissue that protects the root (Sargent and Osborne, 1980; Barrero et al., 2009). Our anatomical description of the pneumatophores indicates that these specialized roots have different zones where the cell layers change in number along with the proximal-distal axes. We also reveal that the function of the developmental regulator SHORT-ROOT is conserved.

Our findings indicate that date palms have developed unique adaptive developmental strategies to survive in the hostile desert environment by protecting their meristems and organs during early development and by orchestrating an efficient growth where the root system is structurally adapted to maximize water uptake and prevent its loss.

RESULTS

Remote germination

In most seed plants species, germination produces a seedling with a discernible shoot and root (Supplemental Figure 1B). In the date palm, this developmental process is described as remote germination during which the seedling develops at a distance from the seed (Demason, 1984; Pinheiro, 2001; Iossi et al., 2006; Henderson, 2006; Baskin and Baskin, 2014) (Supplemental Figure 1A). To characterize this remote germination process, we first monitored date palm growth from germination to the seedling stage (Figure 1). Our macroscopic analysis combined with non-invasive X-ray micro-computed tomography (XμCT) revealed that, in date palms, germination occurs in two phases. First, the cotyledonary petiole emerges and develops away from the seed coat during the first few weeks after germination (Figure 1A-F, Supplemental

Movie 1). Later, the first leave or plumule appears through a protrusion from the cotyledonary petiole (Figure 1G-J). These results suggest that in date palm, organogenesis occurs within the cotyledonary petiole.

To validate these observations, we analyzed the cellular structures of the embryo isolated from the seed (Stage 0) and within the cotyledonary petiole at different stages after emergence (Stage I-III). Interestingly, we found no anatomical differences between Stage 0 and Stage I, confirming that during these stages, embryo development was paused (Figure 2A-K). At Stages II and III the embryo growth is resumed, resulting in a small seedling encapsulated within the cotyledonary petiole and where the root and shoot meristems and developing leaf primordia are morphologically and spatially distinguished (Figure 2L-Q). Later in development, the cotyledonary petiole tip/radicle elongates forming the main root (Figure 3A-D).

Next, we sought to determine whether the encapsulated seedling (Stage II-III) displayed structures with root and shoot characteristics. In plant roots, the columella layers accumulate starch granules, allowing the positioning of the stem cell niche (Dolan et al., 1993; Scheres et al., 1994; Kirschner et al., 2017). Starch granules, together with auxin accumulation at the distal tip, play a key role in sensing and directing a root's responses to gravity (Sabatini et al., 1999; Ottenschlager et al., 2003). In date palms, we found an accumulation of starch granules at the distal root tip of the cotyledonary petiole (Figure 4A-C). This accumulation occurred with high mRNA levels of the auxin response gene *INDOLE-3-ACETIC ACID INDUCIBLE 2* (Swarup et al., 2007) (*PdIAA2*) in the differentiated columella cells, consistent with the auxin maxima present at the distal tip (Figure 4D-F).

The NAC domain gene *SOMBRERO* (*SMB*) also marks the mature columella cells in Arabidopsis and has been described to control the division rates and the orientation of the cell division plane of the columella and epidermis/lateral root cap stem cells (Willemsen et al., 2008). Similarly, we detected *PdSMB* in the differentiated columella layers and the root cap region of the cotyledonary petiole (Figure 4G-I). These data indicate that the distal tip of the cotyledonary petiole exhibited root tip characteristics.

We also assessed whether the shoot identity genes were expressed at the apical pole of the encapsulated seedling. mRNA of the date palm ortholog for *SHOOT MERISTEMLESS* (Long et al., 1996) (*PdSTM*) was confined to the apical region that coincides anatomically with the SAM (Figure 4J-L), whereas the *CUP-SHAPED COTYLEDON 1* ortholog (Aida, 1997)

(*PdCUC1*) mRNA was detected at the boundary between the SAM and the emerging leaf primordia (Supplemental Figure 2A-C). The *AINTEGUMENTA* gene (Mudunkothge and Krizek, 2012) (*PdANT*) was expressed in the SAM and developing leaves (Supplemental Figure 2D-F).

Protective organogenesis in date palm

Our initial observations revealed that the growing cotyledonary petiole contained an embryo with paused growth that resumed development a few weeks after emerging from the seed. To evaluate these developmental dynamics, we monitored the division rates from Stage I to III using ethynyl deoxyuridine (EdU), which incorporates into newly synthesized DNA and can be monitored by a fluorescent dye (Cruz-Ramírez et al., 2013). At Stage I, fluorescence was mainly observed in the tissue layers surrounding the embryo (Figure 5A-C), whereas only a few cells in the embryo displayed fluorescence, indicating a low rate of cell division in the embryo (Figure 5P). At Stage II and III, more cells in the embryo showed fluorescence, which correlated with an increase in the frequency of cell division throughout the embryo (Figure 5F-H, P) and the newly developed leaf primordia (Figure 5K-M, P). The surrounding layers continue to divide and grow in response to gravity carrying the embryo away from the seed (Figure 6).

To relate the observed cell division rates to cell cycle activity, we tested the accumulation of mRNA of the cell cycle gene *HISTONE-H4*, which marks the G1/S phase during the cell cycle (Gutierrez, 2009; Kirschner et al., 2017). We found that *PdHISTONE-H4* mRNA accumulated in a few cells of the embryo at Stage I (Figure 5D, E). *PdHISTONE-H4* expression expanded and became evenly distributed throughout the subsequent developmental stages (Figure 5D, E, I, J, N, O). Our data shows that in Stage I growth of the embryo paused (Figure 6A, B). From Stage II onwards, organogenesis took place within the cotyledonary petiole where the growing embryo/young seedling remained attached to the maternal tissue (Figure 6C, D).

Since embryonic dormancy is modulated by growth and stress hormones (Schiesari and O'Connor, 2013, Barbero et al., 2009), we measured hormone levels in the cotyledonary petiole in Stage I and in the seedling, once it had emerged from the cotyledonary petiole, where the root, shoot and surrounding sheet could be easily distinguished and dissected separately (Supplemental Figure 3). In Stage I, we observed high levels of abscisic acid (ABA) (Supplemental Figure 3), which correlates with its role in repressing cell division and inducing embryonic arrest (Barlow and Pilet, 1984; Sondheimer et al., 1968). In the developed seedlings,

we found a significant decrease in ABA in the shoot and cotyledonary petiole, in addition to an increase in gibberellic acid (GA) levels in the roots (Supplemental Figure 3). In both Stage I and the seedlings, we detected an accumulation of the defense hormones salicylic acid (SA) and jasmonic acid (JA) (Supplemental Figure 3).

Comparative transcriptome analysis of embryos and roots shows distinct gene clusters

To identify transcriptional determinants that govern developmental decisions and that confer adaptation to desert conditions, we conducted a comparison of the transcriptomes of date palm embryos and root tissues. RNAseq reads were generated from total RNA isolated from the emerging cotyledonary petiole in Stage I and from root tissues of emerged seedlings. Our cross-comparison of differentially expressed genes (DEGs) between Stage I and the root tips (using a fold-change of >2X and a FDR of < 0.05) revealed 1396 transcripts that were highly and specifically expressed in Stage I, 3351 transcripts that were highly and specifically expressed in root tips and an overlap of 16,966 transcripts observed in both organs (Figure 5Q).

Next, we performed gene ontology (GO) analysis to annotate the function of differentially expressed genes in embryos and roots and we categorized them by their function either in development, biotic/abiotic resistance, or metabolism. We found an enrichment in expression of developmental genes including transcription factor families in the roots compared with those in the embryo (Figure 5R), which is consistent with the paused development in Stage I. Among the highly enriched genes in roots were those coding for Aquaporins (Figure 5S), involved in facilitating water transport and ion movements in response to osmotic stresses (Gambetta et al., 2017). The enrichment of genes involved in responding to bacteria in roots (Figure 5S) reflects the importance of roots associating with bacterial communities, which might have a role in promoting date palm resistance to drought and salinity (Cherif et al., 2015).

Organization of the date palm root meristem

As the date palm root is adapted to the desert environment, we next explored whether this adaptation is evident in the cellular organization of the date palm roots. We first analyzed the root tip of a 7 month old plant and used both Lugol and modified pseudo-Schiff propidium iodide (mPS-PI) (Truernit et al., 2008) stains to visualize starch in the differentiated columella root cells in longitudinal root sections (Supplemental Figure 4A-B, Figure 7A-B). We found that,

above the stained columella layers, three to four cell layers did not contain starch granules and these layers are likely to form the root stem cell niche (SCN, Figure 7A-B, Supplemental Figure 4A-B). EdU staining showed limited cell division rates around the QC region and the differentiated columella cells (Figure 7C-D).

Date palm roots have been described as having multilayered lignified tissues (Drabble, 1903; Granville, 1974; Seubert, 1997). To evaluate precisely the composition of these tissue layers, we performed histochemical analysis in tissue sections (Figure 7E-I, Figure 8). We found that suberin accumulated in the outermost layers (rhizodermis/velamen (r/v), exodermis) and outer cortex (Figure 7E, E', F, F'). Lignin accumulation was only observed in the r/v and exodermis (Figure 7G, G'). The inner layers forming the inner cortex contained larger cells with intercellular air spaces termed aerenchyma (Figure 7E-E"; F, F", G-G"). Within the cortex, we found bundle cells that accumulated suberin and lignin (Figure 7E", F", G"). A single endodermal layer with Casparian characteristics (Figure 7E-E"'; F-F"', G-G"') encircled a vascular system composed of suberized and lignified xylem and phloem cells expressing the vascular gene *PdATHB15* (Figure 7H, I). Cells at the center forming the pith accumulated more suberin than lignin (Figure 7E"', F"', G"'). The accumulation of suberin and lignin in different tissue layers of date palm roots provides an adaptive advantage by preventing water loss and altering ion transport pathways.

A radial gene network is functionally conserved between date palm and Arabidopsis

In *Arabidopsis thaliana,* the cell fate determinant SHR regulates endodermal patterning (Helariutta et al., 2000). To assess whether the SHR orthologue in date palm, *PdSHR*, performs a similar function, we first analyzed the localization of mRNA in its roots by in situ hybridization and found that, like in Arabidopsis and rice, *PdSHR* is transcribed in the vasculature (Figure 7J, K). Furthermore, we also detected *PdSHR* in the endodermis, cortex and fiber cells of older and mature roots (Figure 7J, Supplemental Figure 4D). To assess whether *PdSHR* fulfilled a similar function in endodermal specification, we introduced the *PdSHR* driven by the Arabidopsis *SHR* promoter (*AtpSHR*) in wild-type (WT) and in *shr* mutants lacking the endodermal layer. We found that *AtpSHR:PdSHR* complemented the root length and restored the double layered ground tissue in *shr* mutants (Figure 7L-N). In Arabidopsis, when *SHR* is expressed from the Arabidopsis *SCARECREOW* promoter *AtpSCR*, additional layers are produced in the ground

tissue (Sena, 2004). Similarly, *PdSHR* was also able to produce multiple ground tissue layers in Arabidopsis when expressed from *AtpSCR* (Figure 7O). These data suggest that, despite being phylogenetically distant, the radial patterning network is conserved between date palm and Arabidopsis.

X-ray micro-Computed Tomography reveals geotropic pneumatophores within the root system

To characterize the root system architecture of living date palms non-invasively, we followed its development using XμCT (Figure 9A, Supplemental Movie 1). Time-course CT imaging revealed strongly positive gravitropic growth of the cotyledonary petiole and the later-emerging crown roots. We also observed, in addition to main roots, crown roots, lateral roots and agravitropic tubular polyp-like structures (Figure 9B-J'). These structures are termed pneumatophores (Jost, 1887; Seubert, 1997).

As the pneumatophores showed different root thickness along the proximal-distal axis, we questioned whether these differences resulted from an increase in cell numbers and tissue layers, or from an increase in cell size. Longitudinal and cross-section analysis revealed that along the proximal distal axis, the pneumatophores have zones with distinct widths: the distal tip containing the stem cell niche and the columella layers (Figure 9E', F'). Above this region resides a thick zone consisting of multiple tissue layers (up to 14 layers from outside to inside; Figure 9E-H) containing small cells possibly forming the meristem, a thicker zone with less tissue layers composed of larger cells (up to 11 layers from outside to inside; Figure 9I) and a thinner zone with less layers and larger cells (up to 7 layers from outside to inside; Figure J). We also observed differences in cell size and number within the vascular tissue (Figure 9H'-J'). These data indicate that unlike most plants roots, where the tissue layers are constant along the growth axis, in the pneumatophores both the cell number and the cell size vary along the proximal-distal and radial axes (Figure 9E-J').

Discussion

Our study highlights important strategies used by the date palm to adapt to the desert environment and reports unique adaptive developmental processes. Remote germination (Figure 1) (Demason, 1988, 1984; Iossi et al., 2006; Tillich, 2007) encapsulates the growing embryo

within the growing cotyledonary petiole that penetrates the soil, deeply burying the meristems and the newly formed organs. This remarkable developmental program protects the future seedlings from the harsh surrounding desert environment. Furthermore, the embryo development pauses during early germination. This phenomenon is reminiscent of some Drosophila species, where photoperiod-mediated reproductive diapause/dormancy in late summer induces the arrest of ovarian development in females at a specific stage. Reproductive development then continues when days become longer and warmer in spring (Salminen et al., 2015).

Our XμCT imaging, combined with tissue sections at different stages, revealed that in date palms, seedlings are encapsulated during early development and form organs while remaining connected to the maternal tissue through the vasculature to provide the water and nutrients necessary to sustain the embryo until emergence (Figure 6). Our data suggest that this process is modulated, at least in part by hormone homeostasis, illustrated by the increased levels of ABA. Elevated levels of ABA are associated with postponed growth in the early stage, while later stages contain more GA, a phytohormone involved in promoting growth during root development (Supplemental Figure 3). Collectively, our data reflect a mechanism of adaptation to the external environment whereby the embryo and the developing seedlings protect their meristems mechanically and molecularly from heat, drought, and pathogens.

The Arabidopsis root has a single endodermal layer, the formation of which is tightly controlled by confining the movement of the transcription factor SHR to the endodermis (Nakajima et al., 2001; Long et al., 2015). Our data show that the date palm ortholog, *PdSHR*, was sufficient to rescue the Arabidopsis *shr* mutants and was able to produce extra layers when expressed under the *SCARECROW* promoter (Figure 7L-O). These observations indicate that the network controlling root radial patterning is conserved not only in rice (*Oryza sativa*) and Arabidopsis, but also distant species like the date palm. Interestingly, analysis of *PdSHR* expression in date palm roots revealed a broader expression domain as the mRNA accumulated in the endodermis and the vasculature, and a subset of cells in the cortex including the fiber bundles in the date palm roots. This expression suggests that *PdSHR* function might not be restricted to the specification of the endodermis, and may include fiber-cell specification. These fibers display similar features to the vascular tissue, including suberin accumulation and SHR expression, which could imply a function in maximizing efficient water transport and aiding in preventing water loss.

Our XμCT imaging during date palm root development revealed secondary roots similar to lateral roots, and a subset of roots, the pneumatophores, with different diameters along their longitudinal axis growing either horizontally or upwards against gravity (Figure 9A, B) (Jost, 1887; Granville, 1974; Seubert, 1997). Our imaging showed that the number of cell layers is not constant along the longitudinal axis, and the difference in cell size and cell layers between the different regions of the pneumatophore suggests a different mechanism for the longitudinal zonation pattern when compared to classical lateral roots (Figure 9E-F', H-J'). One plausible explanation is that the decrease of the layers at the proximal zone might be due to the detachment of the outer layers as the root grows away from the meristem. Another scenario might involve distinct hormone distribution between the zonation leading to this difference in cell size and tissue layers. Pneumatophores can also be found in many other species including mangrove plants (Yampolsky, 1924), where they contribute to root respiration. It remains to be determined whether pneumatophores have a similar role in date palms. Plausibly, these structures are used to increase the spatial distribution of the roots, which allows not only efficient colonization of the soil area but also maximizes water uptake during sporadic and unexpected rainfall in the desert. During such rainfall events, the pneumatophores, growing near the soil surface, would increase root water uptake, while water retention within the main root would be carried out by the suberized outer layers and fiber cells. Understanding the molecular and hormonal mechanisms of pneumatophore formation and function will be useful to engineer crops that can efficiently manage water uptake.

The observed structures in root tissues account for the adaptation of date palms to drought and high salinity. Highly suberized and lignified tissue layers provide an advantage in balancing ion fluxes and monitoring the passage of ions through the vasculature. Furthermore, our transcriptomic data show an enrichment of Aquaporins (Figure 5S) in root tissue, which is consistent with their role in promoting root water uptake (Tyerman et al., 2017; Gambetta et al., 2017). We also observed an enrichment in genes involved in response to bacteria. This reflects the importance of root-associated bacterial communities, which have been reported to facilitate nutrient uptake and promote resistance to drought and salinity in date palms (Cherif et al., 2015). It would be attractive to decipher how the date palm microbiome influences the developmental programs and contributes to these adaptive strategies.

Our data reveal a unique developmental plasticity in date palms that allows them to adapt to their arid environment. Revealing these developmental adaptations provides important foundational knowledge not only for the development of desert agriculture, but also has a potential for generating crops with an optimized and efficient root system and an increased stress tolerance, which will be essential as the world faces rapid global climate changes.

METHODS

Date palm seed sterilization and germination

Date palm (*Phoenix dactylifera*) seeds were sterilized by washing with detergent (20% in water) for 15 min followed by o/n stratification using 20% sulphuric acid. The seeds were then washed with sterile water and sterilized with 10% chlorine bleach for 20 min followed by extensive washing with sterile water. The sterilized seeds were plated in ½-strength Murashige and Skoog medium containing 0.05% (w/t) morpholinoethanesulfonic acid monohydrate (pH 5.7), 1.0% sucrose, and 0.8 % plant agar and germinated at 32°C in dark.

Tissue sections, staining, and microscopy

Fresh samples were embedded in agarose and sectioned either by hand or by using a Leica VT1000S vibratome. SCRI Renaissance 2200 (SR2200) (Musielak et al., 2015) stain was used to visualize cell walls while berberine hemisulfate stain was used to visualize suberin and lignin (Musielak et al., 2015). Sections were imaged using an LSM 710 upright confocal microscope with excitation of 405 nm for SCRI or 488 nm for berberine.

Lignin staining was performed using Phloroglucinol HCl as described in (Hofhuis et al., 2016); images were taken using an Olympus BX41 upright brightfield microscope. For longitudinal sections, fresh samples were embedded in 13% low melting agar and sectioned. Lugol was used to visualize starch granules. Samples were mounted in Visikol optical clearing agent and analyzed by an Olympus BX41 upright brightfield microscope.

mPS-PI staining was performed as (Truernit et al., 2008). PI was excited with a 561 nm Argon laser with emission detection at 566–718 nm.

Microtome plastic section: Samples were fixed under vacuum for 48 hours with 4% paraformaldehyde (w/v), 5% glutaraldehyde (v/v) in 50 mM phosphate buffer (pH 7.2). Tissue processing and embedding for plastic and paraffin sectioning were carried out as described in

(Long et al., 2015). Root sections were made using a RJ2035 microtome (Leica Microsystems) and stained in ruthenium red for 10 min, and then mounted in Depex. Images were captured with a Normaski microscope (Axio Imager; Carl Zeiss, DM5500B microscope).

EdU staining for cell proliferation analysis

Cell division rates in date palm seedlings were evaluated using the Click-iT® EdU Alexa Fluor® 488 Imaging Kit (C10637 Invitrogen), as described in (Cruz-Ramirez et al., 2013). Samples were incubated with EdU diluted in MS for 24 h and then fixed in 3.7% formaldehyde for 1 h under vacuum, and then sectioned by vibratome. Sections were permeabilized with PBS containing 0.5% Triton X-100 for 1 h and incubated for 1 h in the dark with a "click-it-reaction cocktail", which was prepared according to the manual, followed by DNA-counterstaining using Hoechest 33342 in PBS under vacuum in the dark for 1 h. Sections were mounted in clearing solution and incubated in the dark for 2 weeks at 4 °C as described in (Kirschner et al., 2017). Images were captured by Zeiss LSM 710 inverted confocal microscope.

Image acquisition

To obtain high resolution images from large date palm samples, several images were taken from the same sample and a full image was reconstituted. In the confocal, images were acquired using the tile scan function in the Zen software with automatized stitching. Regions of interest were divided into multiple tiles and imaged individually. The tiles were then combined via automatic stitching to create a large overview image. Images acquired using light microscope were stitched using the Photomerge function in Adobe Photoshop CC 2018.

RNA in situ gene expression assays

In situ hybridization was performed using microtome for either tissue sections as described in (Carlsbecker et al., 2010), or a whole mount protocol using vibratome sections. Date palm sequences were retrieved either from NCBI database based on homology with Arabidopsis, or from the obtained RNAseq dataset. Probes were amplified from cDNA synthesized from date palm seedlings using the primers listed in Table 1 and cloned into the pGEM-T vector (Promega). Probe synthesis was performed as described in (Blilou et al., 2002). Samples were imaged using a Leica DM2500 LED stand.

Hormone measurements from date palm tissues

Phytohormones were quantified according to (Delatorre et al., 2017), with the following modifications. Approximately 10 mg of freeze-dried ground tissues were used for the measurements. The internal standards D6-ABA (0.42 ng), D2-GA1 (0.04 ng), D4-SA (0.05 ng), and D2-JA (0.74 ng) were spiked into the ground tissues along with 1.5 mL of methanol. The mixture was sonicated for 15 min in an ultrasonic bath (Branson 3510), followed by centrifugation for 10 min at 14,000 rpm at 4 °C. The supernatant was collected and the pellet was re-extracted with 1.5 mL of the same solvent. Then, the two supernatants were combined and dried under vacuum. The sample was redissolved in 150 µL of acetonitrile-water (25:75, v:v) and filtered through a 0.22 µm filter for LC-MS analysis. Plant hormones were analyzed using HPLC-Q-Trap-MS/MS with MRM mode. Chromatographic separation was achieved on a ZORBAX Eclipse plus C18 column (150 × 2.1 mm; 3.5 µm; Agilent). Statistical analysis was performed using one-way ANOVA and Tukey's post-hoc test.

X-ray micro-computed tomography imaging

X-ray micro-computed tomography imaging of germinated date palm seedlings (Stage I) was carried out using a Nikon XT H 225 (Nikon Metrology, Leuven, Belgium) device with a Paxscan 2520DX X-ray amorphous-Si flat panel detector (Varian Imaging Systems, Palo Alto, CA, USA). The XµCT device was set to operate at a voltage and current of 60kV and 100µA, respectively. The date palm sample was scanned at a voxel size resolution of 12 µm, with the specimen stage rotating through 360 degrees at a rotation step increment of 0.115 degrees over a period of approximately 2 h, such that a total of 3141 projection images were obtained by averaging 8 frames with an exposure of 250 ms each, at every rotation step. The software CT Pro 3D 4.4.2 (Nikon Metrology, Hertfordshire, United Kingdom) was used to perform the reconstruction of the projection images, resulting in 1524 slice images with a resolution of 1910 x 1910 pixels each. A volume rendering and analysis software (Avizo 9.2.0, FEI Company, Hillsboro, Oregon, USA) was used to render images from the 3D dataset.

The monitoring of date palm developmental stages was performed on a Phoenix V|TOME|X M 240 high-resolution X-ray CT system (GE Sensing and Inspection Technologies, Wunstorf, Germany) at the Hounsfield Facility, University of Nottingham, UK. The scanning parameters were optimized to allow a balance between a large field of view and high-resolution. The same

sample was imaged at consecutive time points over 11 months. Each time, the sample was scanned with a voltage and current of 160kV and 180µA, respectively, at a voxel size resolution of 40 µm, with the specimen stage rotating 360 degrees at a rotation step increment of 0.166 degrees over a period of approximately 3 hours. A total of 2160 projection images were obtained by averaging 3 frames with an exposure of 250 ms each, at every rotation step. Due to the height of the cylinder (40 cm), 5 separate scans were made to cover and image the entire height of the sample. Each sub-scan was then reconstructed using DatosRec software (GE Sensing and Inspection Technologies, Wunstorf, Germany) and then manually combined in VG Studio MAX v2.2 (Volume Graphics GmbH, Heidelberg, Germany) and exported as a single 3D volumetric dataset. To distinguish the phases of the root system from the soil material, image processing techniques were applied by segmenting the reconstructed CT data using a region-growing method in VG Studio MAX v2.2.

Date palm transcriptomics

Date palm RNA extraction

Stage I cotyledonary petiole and germinated root tips (from 12-week-old seedlings) were sampled for RNA extraction. The total RNA was extracted from 75 mg (root tips) and 200 mg (embryo) of plant material. The tissue was ground at -80 ºC using liquid nitrogen immediately after collection. RNA isolation was carried out by using TRIzol Reagent (15596026 - Ambion) according to the manufacturer's specifications. The total RNA was treated with DNAse I. RNA concentration and quality was measured by using Nanodrop and a 1.5% agarose electrophoresis gel.

RNAseq library generation and sequencing

The starting material for RNA sequencing was of 10 µg of RNA per sample. Two biological replicates were used per sample. Libraries and sequencing were generated at the Genomic Advanced Unit-LANGEBIO sequencing facilities. Four independent libraries using TruSeq protocols were processed and were sequenced on a 2 x 150 platform according to the manufacturer’s instructions and recommendations.

The four libraries were sequenced in a 2 x 150 format using Illumina NextSeq platform. 47,435,916 and 49,260,416 paired end reads for the embryos and 48,058,648 and 52,789,080 paired end reads for the root were obtained (Supplemental Table 2). All reads passed our quality

filters and were used in the subsequent analyses. Raw data were deposited in NCBI SRA under accession PRJNA497070 and can be traced on: https://www.ncbi.nlm.nih.gov/sra/?term=PRJNA497070.

Transcript assembly and annotation

rnaSPAdes v1.0.0 (present in SPAdes v3.9) were used to reconstruct the date palm transcriptome. Samples were combined and assembled using default parameters in rnaSPAdes. The final assembly was annotated by first identifying their main open reading frame (ORF) and then comparing the peptide sequence with the NCBI Non-Redundant database (downloaded Nov. 2015) with Blast+ v2.2.30 and then retaining the best match with E-value < 1 e-6.

The resulting transcriptome contained 110,808 sequences longer than 300 bp with an average size of 1079 bp and a maximal length of 16,237 bp of a sequence corresponding to the gene LONGIFOLIA 1. In addition, 42,418 non-redundant mRNA ORFs and 218,325 non-coding sequences were found.

Differentially expressed genes in embryos

Transcript quantification was obtained using each Kallisto library separately with a bootstrap of 1000. The embryo differentially expressed genes were detected using R: Bioconductor package EdgeR.

Accession Numbers

The *Phoenix dactylifer*a cDNA accessions used in this study are as follows: LOC103704820 (*PdSOMBRERO*); LOC103708475 (homeobox-leucine zipper protein: *pdATHB-15*); LOC103705495 (NAC domain-containing protein 78 similar to *PdCUC1*), LOC103715985 (*PdSHORT-ROOT*); LOC103711557 (homeobox protein knotted-1-like with similarity to *PdSHOOTMERISTEMLESS*), LOC103704533 (auxin-induced protein *PdIAA2*), LOC103710075 (*PdHISTONE H4-1*).

Supplemental Data

Supplemental Figure 1. Germination modes in palms and rice.

Supplemental Figure 2. Expression analysis of genes marking the shoot meristem and organ primordia.

Supplemental Figure 3. Measurement of hormone contents.

Supplemental Figure 4. Conserved function of date palm *SHORTROOT* in *Arabidopsis thaliana*

Supplemental Table 1. Primers used in this study

Supplemental Table 2. RNAseq reads per sample

Supplemental Movie 1. Date palm germination and growth visualized by X-ray micro-computed tomography.

ACKNOWLEDGMENTS

The research reported in this publication was supported by King Abdullah University of Science and Technology (KAUST). We acknowledge awards from the Biotechnology and Biological Sciences Research Council [grant numbers BB/PO16855/1, BB/M001806/1]; European Research Council FUTUREROOTS Advanced Investigator grant 294729; and Leverhulme Trust grant RPG-2016-409"

We thank the manager of Publication Services and Researcher Support (KAUST), Dr. Virginia A. Unkefer and Dr Michael Cusack, for editing and critical reading of the manuscript. We are also grateful for the support from the KAUST Core Labs, especially the staff in the Imaging and Characterization Core Lab (https://corelabs.kaust.edu.sa/imaging).

The authors thank Prof. Renze Heidstra for his critical reading of the manuscript.

AUTHOR CONTRIBUTIONS

The scientific concept and the experimental design were developed by IB. IB, TX, YD and GK performed in situ hybridization; IB and TX analyzed the root anatomy of the date palm. AA, JC, and AC performed RNA seq experiments and data analysis. BA, CS, and MB conducted X-ray μCT at different date palm developmental stages. VL and GL conducted X-ray μCT in the early germinated seedlings. VL photographed date palm seedlings. JW and SB contributed with hormone measurements.

Competing financial interests

The authors declare no competing financial interests.

References

Aida, M. (1997). Genes Involved in Organ Separation in Arabidopsis: An Analysis of the cup-

shaped cotyledon Mutant. Plant Cell Online **9**: 841–857.

Al-dous, E.K. et al. (2011). De novo genome sequencing and comparative genomics of date palm (Phoenix dactylifera). Nat. Biotechnol. **29**: 521–527.

Al-Mssallem, I.S. et al. (2013). Genome sequence of the date palm Phoenix dactylifera L. Nat. Commun. **4**: 1–9.

Apfeld, J. and Kenyon, C. (1998). Cell nonautonomy of C. elegans daf-2 function in the regulation of diapause and life span. Cell **95**: 199–210.

Barlow, P.W. and Pilet, P.E. (1984). The effect of Abscisic acid from cell growth, cell division and DNA synthesis in the maize root meristem. Physiol. Plant. **62**: 125–132.

Barrero, M., Talbot, M.J., White, R.G., Jacobsen, J. V, and Gubler, F. (2009). Anatomical and Transcriptomic Studies of the Coleorhiza Reveal the Importance of This Tissue in Regulating Dormancy in Barley. **150**: 1006–1021.

Baskin, J.M. and Baskin, C.C. (2014). What kind of seed dormancy might palms have ? Seed Sci. Res.: 17–22.

Blilou, I., Frugier, F., Folmer, S., Serralbo, O., Willemsen, V., Wolkenfelt, H., Eloy, N.B., Ferreira, P.C.G., Weisbeek, P., and Scheres, B. (2002). The Arabidopsis HOBBIT gene encodes a CDC27 homolog that links the plant cell cycle to progression of cell differentiation. Genes Dev. **16**: 2566–2575.

Carlsbecker, A. et al. (2010). Cell signalling by microRNA165 / 6 directs gene dose-dependent root cell fate. **465**.

Cherif, H. et al. (2015). Oasis desert farming selects environment-specific date palm root endophytic communities and cultivable bacteria that promote resistance to drought. Environ. Microbiol. Rep. **7**: 668–678.

Cruz-Ramírez, A., Díaz-Triviño, S., Wachsman, G., Du, Y., Arteága-Vázquez, M., Zhang, H., Benjamins, R., Blilou, I., Neef, A.B., Chandler, V., and Scheres, B. (2013). A SCARECROW-RETINOBLASTOMA Protein Network Controls Protective Quiescence in the Arabidopsis Root Stem Cell Organizer. PLoS Biol. **11**.

Delatorre, C., Rodríguez, A., Rodríguez, L., Majada, J.P., Ordás, R.J., and Feito, I. (2017). Hormonal profiling: Development of a simple method to extract and quantify phytohormones in complex matrices by UHPLC–MS/MS. J. Chromatogr. B Anal. Technol. Biomed. Life Sci. **1040**: 239–249.

Demason, D. (1984). Growth Parameters in the Cotyledon of Date Seedling. Bot. Gaz. **145**: 176–183.

Demason, D. (1988). Seedling Development in Washingtonia filifera. Bot. Gaz. **149**: 45–56.

Dolan, L., Janmaat, K., Willemsen, V., Linstead, P., Poethig, S., Roberts, K., and Scheres, B. (1993). Cellular organisation of the Arabidopsis thaliana root. Development **119**: 71–84.

Drabble, E. (1903). On the anatomy of the roots of palms. Botany: 48–51.

Dreyer, B., Morte, A., López, J.Á., and Honrubia, M. (2010). Comparative study of mycorrhizal susceptibility and anatomy of four palm species.: 103–115.

Fenelon, J.C., Banerjee, A., and Murphy, B.D. (2014). Embryonic diapause: Development on hold. Int. J. Dev. Biol. **58**: 163–174.

Fielenbach, N. and Antebi, A. (2008). C. elegans dauer formation and the molecular ba1. S. Y. Park, M. Tong, and J. L. Jameson. Genes Dev. **22**: 2149–65.

Fls, P.B.T. (2006). The uniqueness of palms.: 5–14.

Gambetta, G.A., Knipfer, T., Fricke, W., and Mcelrone, A.J. (2017). Plant Aquaporins.: 133–153.

Granville (1974). Aperçu sur la structure des pneumatophores de deux espèces des sols hydromorphes en Guyane Centre ORSTOM de Cayenne. cah ORSTOM **23**: 3–22.

Gutierrez, C. (2009). The Arabidopsis Cell Division Cycle. In The Arabidopsis Book, pp. 1–19.

El Hadrami, F. Daayf, S. Elshibli, S.M. Jain, and I.E.H. (2011). Date Palm Genetics and Breeding. In Date Palm Biotechnology, pp. 479–512.

Hazzouri, K.M. et al. (2015). Whole genome re-sequencing of date palms yields insights into diversification of a fruit tree crop. Nat. Commun. **6**.

Helariutta, Y., Fukaki, H., Wysocka-Diller, J., Nakajima, K., Jung, J., Sena, G., Hauser, M.T., and Benfey, P.N. (2000). The SHORT-ROOT gene controls radial patterning of the Arabidopsis root through radial signaling. Cell **101**: 555–567.

Henderson, F.M. (2006). Morphology and Anatomy of Palm Seedlings. **72**: 273–329.

Hofhuis, H. et al. (2016). Morphomechanical Innovation Drives Explosive Seed Dispersal. Cell **166**: 222–233.

Iossi, E., Moro, F.V., and Sader, R. (2006). Seed anatomy and germination of Phoenix roebelenii (Arecaceae). Rev. Bras. Sementes **28**: 121–128.

Jost, L. (1887). Ein Beitrag zur Kenntniss der Athmungsorgane der Pflanzen.

Kirschner, G.K., Stahl, Y., Von Korff, M., and Simon, R. (2017). Unique and Conserved Features of the Barley Root Meristem. Front. Plant Sci. **8**.

Liu, Z., Xin, Y., Zhang, Y., Fan, J., and Sun, J. (2016). Summer diapause induced by high temperatures in the oriental tobacco budworm: Ecological adaptation to hot summers. Sci. Rep. **6**: 2–11.

Long, J.A., Moan, E.I., Medford, J.I., and Barton, M.K. (1996). A member of the KNOTTED class of homeodomain proteins encoded by the STM gene of Arabidopsis. Nature **379**: 66–69.

Long, Y., Smet, W., Cruz-Ramírez, A., Castelijns, B., de Jonge, W., Mähönen, A.P., Bouchet, B.P., Perez, G.S., Akhmanova, A., Scheres, B., and Blilou, I. (2015). Arabidopsis BIRD Zinc Finger Proteins Jointly Stabilize Tissue Boundaries by Confining the Cell Fate Regulator SHORT-ROOT and Contributing to Fate Specification. Plant Cell **27**: tpc.114.132407.

Marondedze, C., Gehring, C., and Thomas, L. (2014). Dynamic changes in the date palm fruit proteome during development and ripening. Hortic. Res. **1**: 1–15.

Mosqueira, M.J., Marasco, R., Fusi, M., Michoud, G., Merlino, G., Cherif, A., and Daffonchio, D. (2019). Consistent bacterial selection by date palm root system across heterogeneous desert oasis agroecosystems.: 1–12.

Mudunkothge, J.S. and Krizek, B.A. (2012). Three Arabidopsis AIL/PLT genes act in combination to regulate shoot apical meristem function. Plant J. **71**: 108–121.

Musielak, T.J., Schenkel, L., Kolb, M., Henschen, A., and Bayer, M. (2015). A simple and versatile cell wall staining protocol to study plant reproduction. Plant Reprod. **28**: 161–169.

Nakajima, K., Sena, G., Nawy, T., and Benfey, P.N. (2001). Intercellular movement of the putative transcription factor SHR in root patterning. Nature **413**: 307–311.

Ottenschlager, I., Wolff, P., Wolverton, C., Bhalerao, R.P., Sandberg, G., Ishikawa, H., Evans, M., and Palme, K. (2003). Gravity-regulated differential auxin transport from columella to lateral root cap cells. Proc. Natl. Acad. Sci. **100**: 2987–2991.

Pinheiro, C.U.B. (2001). Germination Strategies of Palms. New York Bot. Gard. **53**: 519–527.

Sabatini, S., Beis, D., Wolkenfelt, H., Murfett, J., Guilfoyle, T., Malamy, J., Benfey, P.N., Leyser, O., Bechtold, N., Weisbeek, P., and Scheres, B. (1999). An Auxin-Dependent Distal Organizer of Pattern and Polarity in the *Arabidopsis* Root. Cell **99**: 463–472.

Salminen, T.S., Vesala, L., Laiho, A., Merisalo, M., Hoikkala, A., and Kankare, M. (2015). Seasonal gene expression kinetics between diapause phases in Drosophila virilis group species and overwintering differences between diapausing and non-diapausing females. Sci. Rep. **5**: 1–13.

Sargent, J.A. and Osborne, D.J. (1980). Root Cells During the Early Hours of Germination of Rye Embryos. Protoplasma **103**: 91–103.

Scheres, B., Wolkenfelt, H., Willemsen, V., Terlouw, M., Lawson, E., Dean, C., and Weisbeek, P. (1994). Embryonic origin of the Arabidopsis primary root and root meristem initials. Development **120**: 2475–2487.

Schiesari, L. and O'Connor, M.B. (2013). Diapause. Delaying the developmental clock in response to a changing environment. In Current Topics in Developmental Biology, pp. 213–246.

Sena, G. (2004). A broad competence to respond to SHORT ROOT revealed by tissue-specific ectopic expression. Development **131**: 2817–2826.

Seubert, E. (1997). Root anatomy of palms: I. Coryphoideae. Flora **192**: 81–103.

Seubert, E. (1996). Root anatomy of palms Desription of the roots. **107**: 43–59.

Sondheimer, E., Tzou, D.S., and Galson, E.C. (1968). Abscisic Acid levels and seed dormancy. Plant Physiol. **43**: 1443–7.

Stephan, N., Halama, A., Mathew, S., Hayat, S., Bhagwat, A., Mathew, L.S., Diboun, I., Malek, J., and Suhre, K. (2018). A comprehensive metabolomic data set of date palm fruit. Data Br. **18**: 1313–1321.

Swarup, R., Perry, P., Hagenbeek, D., Straeten, D. Van Der, Beemster, G.T.S., Bhalerao, R., Ljung, K., and Bennett, M.J. (2007). Ethylene Upregulates Auxin Biosynthesis in Arabidopsis Seedlings to Enhance Inhibition of Root Cell Elongation. **19**: 2186–2196.

Tillich, H.J. (2007). Seedling diversity and the homologies of seedling organs in the order Poales (monocotyledons). Ann. Bot. **100**: 1413–1429.

Truernit, E., Bauby, H., Dubreucq, B., Grandjean, O., Runions, J., Barthélémy, J., and Palauqui, J.-C. (2008). High-resolution whole-mount imaging of three-dimensional tissue organization and gene expression enables the study of Phloem development and structure in Arabidopsis. Plant Cell **20**: 1494–1503.

Tyerman, S, Wignes, A, and Kaiser, B. and Role (2017). Root Hydraulic and Aquaporin

Responses to N Availability. In Plant Aquaporins From Transport to Signaling, pp. 207–237.

Wadsworth, C.B., Woods, W.A., Hahn, D.A., and Dopman, E.B. (2013). One phase of the dormancy developmental pathway is critical for the evolution of insect seasonality. J. Evol. Biol. **26**: 2359–2368.

Welch, D., Hassan, H., Blilou, I., Immink, R., Heidstra, R., and Scheres, B. (2007). Arabidopsis JACKDAW and MAGPIE zinc finger proteins delimit asymmetric cell division and stabilize tissue boundaries by restricting SHORT-ROOT action. Genes Dev. **21**: 2196–2204.

Willemsen, V., Bauch, M., Bennett, T., Campilho, A., Wolkenfelt, H., Xu, J., Haseloff, J., and Scheres, B. (2008). The NAC Domain Transcription Factors FEZ and SOMBRERO Control the Orientation of Cell Division Plane in Arabidopsis Root Stem Cells. Dev. Cell **15**: 913–922.

Yampolsky, C. (1924). The Pneumathodes on the Roots of the Oil Palm (Elaeis guineensis Jacq .). Am. J. Bot. **11**: 502–512.

Figure legends

Figure 1. The germination process in date palms. (A-F) 2-4 weeks after germination; (G) 8 weeks after germination, (H) 10 weeks after germination and (I-J) 12 weeks after germination. A, C, E and G-I are macrophotographs. B, D, F and J are images obtained from 3D X-ray computed tomography. The white arrows in G and H point to tissue apertures allowing leaves to emerge; purple arrowheads point to the cotyledonary petiole (CP). Abbreviations: w, weeks after germination. The scale bars are 1 cm. Images are representative of 40 seedlings.

Figure 2. Growth dynamics during germination in date palms. (A) Date palm seed containing the embryo. (B) Embryonic sac dissected from the seed (n= 20). (C, D) Longitudinal section of dissected embryo sac stained with modified pseudo-Schiff propidium iodide (mPS-PI) (n=20). The white arrows indicate root and shoot axes in C. (E, F) 3D image of germinated date palm at Stage I imaged with XμCT (n=3). (G,H) Confocal images of cotyledonary petiole sections taken

at the same stage as F. The section in (G) at the upper part, which does not include the embryo; the section in (H) includes a transverse view of the embryo (n=15). (I-Q) Date palm growth at 1-4 weeks after germination (n=25). I, L, and O are macrophotographs; J, K, M, N, P, and Q are confocal images of longitudinal vibratome sections with the cell walls stained with SCRI Renaissance 2200 (n=10). White arrowheads point to the vasculature (Vas); purple arrowheads point to the cotyledonary petiole (CP). The black arrows in H and J indicate the embryo. Abbreviations: RP, root pole; SP, shoot pole; SAM, shoot apical meristem; LP, leaf primordia; RAM, root apical meristem; CPT, cotyledonary petiole tip. D, K, N, and Q are insets of C, J, M and P, respectively. The scale bars indicate: A, 1 cm; B, 0.5 cm; C and D, 100 µm; E, 5 mm; F, 2 mm; G, C and H, 100 µm; I, L, and O, 1 cm; G, M, and P, 100 µm; K, N and P, 50 µm. Images are representative of the total number (n) of seedlings that were studied.

Figure 3. Encapsulated organogenesis in date palms. (A-C) Confocal images of 4-6 weeks longitudinal sections of date palm stained with mPS-PI. (D) DIC images of the longitudinal plastic section stained with Toluidine blue O. Abbreviations: RAM, root apical meristem; SAM, shoot apical meristem; ESJ, root-shoot junction; Vas, vasculature; CPT, cotyledonary petiole tip; w, weeks after germination. Scale bars indicate 100 µm. Images are representative of 10 seedlings that were studied.

Figure 4. Characterization of root and shoot meristem in date palms. (A-C) Accumulation of starch granules at the root tip. Light microscope images of vibratome sections stained with Lugol (A, B; n=8; brown color). Plastic longitudinal sections stained with ruthenium red (pink color) and Lugol (C; n=8). (D-F) Gene expression analysis with in situ hybridization using the date palm auxin response gene *IAA2* (*PdIAA2*); antisense probe (D, E; n=15; mRNA signal is shown in blue/purple); sense control (F; n=15). (G-I) Differentiated columella layers are marked with date palm *SOMBRERO* (*PdSMB*). The antisense probe (G, H; n=10; mRNA signal is shown in brown) is compared with the sense control for *PdSMB* (I; n=10). (J-L) The shoot meristem is marked with *SHOOT MERISTEMLESS* gene *STM* (*PdSTM*), the antisense probe (J, K; n=9; mRNA signal is shown in brown); sense control for *PdSTM* (L; n=9). E, H, K are zoomed in from D, G, J respectively. Abbreviations: SCN, stem cell niche; SG, starch granules; CPC, cotyledonary petiole cap; SAM, shoot apical meristem; LP, leaf primordia; RAM, root apical

meristem. Scale bars indicate: A and C, 50 µm; D-F, 100 µm; G, I, J, and L, 200 µm; H, 100 µm; K, 50 µm. Images are representative of the total number (n) of seedlings that were studied.

Figure 5. Postembryonic development correlates with an increase in cell division rates and activation of developmental genes. (A, F, K) Cartoons representing the early developmental stages of date palms, Stage I (A-E), Stage II (F-J) and Stage III (K-O). (B, C, G, H, L, M). Confocal images of vibratome sections from the cotyledonary petiole showing dividing cells as captured by EdU staining (n= 35). Dividing EdU stained nuclei are shown in green; nuclei counterstained with Hoechst 33258 are shown in magenta. C, H and M are inset from B, G, and L, respectively. Scale bars indicate 100 µm. (D, E, I, J, N, O) In situ hybridization showing *PdHistone-H4* expression (n=20; signal is shown in blue/purple color). B-E, G-J, L-O are representative images of the total number (n) of seedlings that were studied. (P) Graph showing cell division rates in different zones and at different developmental stages of the seedlings. The x-axis represents developmental stages and the y-axis represents the measured frequency of cells incorporating EdU. Each column represents the average cell division frequency in a specific zone of the tip of the cotyledonary petiole. Error bars represent the ± standard errors. Numbers (n) of seedlings that were used: Stage I, n=14; Stage II, n=12; Stage III, n=6. Average nuclei counted (Hoechst) for the cell division frequency calculation per stage and per zone represented as follows. Shoot: RAM: dividing columella: root-shoot junction, 604: 210: 342: 97 (Stage I), 557:275:376:105 (Stage II) and 597, 494, 271, 107 (Stage III), respectively. Zones are indicated in colors in (A, F and K): Shoot (green); RAM (orange); dividing columella (pink); root-shoot junction (brown); cotyledonary petiole cap (CPC) (light brown). Measured zones are represented in P. (Q) Venn diagram showing overlapping and differentially expressed genes in Stage I and 12-week-old roots resulting from RNA-seq data. (R) Heat map representation of differentially expressed developmental genes. (S) Selected categories of enriched gene ontology (GO). Up-regulation is shown in red; downregulation is shown in blue.

Figure 6. Schematic representations of date palm development from embryo to forming organs within the cotyledonary petiole. Representations are illustrations from longitudinal sections of real samples. Black arrowhead points to the cotyledonary petiole (CP). Abbreviations: Vas;

753 vasculature, LP; leaf primordia, RSJ; root-shoot junction, QC; quiescent center; CSC; columella
754 stem cells; CPC, cotyledonary petiole cap.
755
756 **Figure 7**. Date palm root anatomy. (A, B) Confocal scanning images of longitudinal sections of
757 roots obtained from 7-month-old plants and stained with mPS-PI (n=3). (C, D) Dividing nuclei
758 are stained with EdU (green) (n=5). Nuclei were counterstained with Hoechst (purple). (E-F’’’)
759 Confocal image of a cross-section of a root stained with SCRI Renaissance 2200. Purple
760 indicates cell wall staining; green is the auto-fluorescence marking lignin and suberin deposition
761 within the roots (E-E’’’). A berberine stained cross-section marks suberin in green (F-F’’’). (G-
762 G’’’) Lignin accumulation in a cross-section stained with Phluoglucocinol in dark brown. (H-K)
763 RNA in situ hybridization in 12-week-old roots. Signal blue/purple shows mRNA localization of
764 vascular *PdATHB15* (H, I) and *PdSHR* (J, K) in date palm roots. Date palm SHR function is
765 conserved in Arabidopsis. (L-O) Confocal images of a root stained with Propidium Iodide of
766 At*pSHR:PdSHR* in WT (L; n=6); *shr* mutant (M; n=6); At*pSHR:PdSHR* in *shr* (N; n=8) and
767 *AtpSCR:PdSHR* in WT (O; n=6). B, D, E’-E’’’, F’-F’’’, G’-G’’’ I and K show zoomed images
768 from A, C, E, F, G, H and J, respectively. Abbreviations: SCN, stem cell niche; Col, columella;
769 Vas, vasculature; R/V, rhizodermis/velamen; Ex, exodermis; OC, outer cortex; IC, inner cortex;
770 En, endodermis; CS, Casparian strips; Mx, metaxylem; Ph; phloem; X, xylem; Ae, aerenchyma;
771 FC, fiber cells; Ep, Epidermis; GT, Ground tissue: cortex and endodermis, Sn, supernumerary
772 layers. The scale bars indicate 100 μm in A, C, E, F, G, H and J; 50 μm in B, D, E’-E’’’, F’-F’’’,
773 G’-G’’’, I and K; 20 μm in L-O. Images are representative of the total number (n) of roots that
774 were studied.
775
776 **Figure 8.** Schematic representation of the date palm root. (A) Longitudinal section, (B) cross
777 section. Colors represent distinct tissue types. Abbreviations: R/V: rhizodermis/velamen; Ex,
778 exodermis; OC: outer cortex; IC, inner cortex; Ae, aerenchyma; FC, fiber cells; En, endodermis;
779 Per, pericycle; Ph; phloem; X, xylem; Vas, vasculature; Col+LRC, columella and lateral root
780 cap; CSC, columella stem cells; QC, quiescent center.
781
782 **Figure 9**. Characterization of date palm pneumatophores. (A, B) X-ray micro-computed
783 tomography images showing the root system architecture of the date palm: the primary root with

secondary lateral horizontal growth and aerial roots with upward vertical growth. (B) is a zoomed image of A. (C, D, G) micrographs showing pneumatophores (n=10). (E, E') Longitudinal sections of date palm pneumatophores stained with mPS-PI (n=5). (F, F') DIC images of sections stained with Toluidine blue O (n=5). (H-J') Cross-sections of different zones within the pneumatophore (n=5); basal thin region (white arrowhead; H, H'), basal thick region (purple arrowhead; I, I') and apical thin region (black arrowhead; J, J'). E' F' H', I', and J' are enlargements of E, F, H, I, and J respectively. Abbreviations: MR, main root, CR, crown root. The scale bars indicate: A, 20 mm; B, 4.5 mm; C, D, G, 1 cm; E, F, 100 μm; H, I, J, E', F' 50μm; H', I', J' 25 μm. Images are representative of the total number (n) of roots that were studied.

Supplemental Figures and Tables

Supplemental Figure 1. Germination modes in palms and rice. (A) Schematic representation of the different modes of germination in palms adapted from (Henderson, 2006). (B) Macrograph showing rice 1, 2, and 3 days after germination (B; n=10). The scale bar in B is 1 cm.

Supplemental Figure 2. Expression analysis of genes marking the shoot meristem and organ primordia. In situ hybridization in a tissue section using gene delimiting organ boundaries *CUP-SHAPED COTYLEDON* (*PdCUC*) and primordial gene *AINTEGUMENTA* (*PdANT*). A, B, D, E are antisense probes (n=8), whereas C (n=5), F (n=7) are sense probes. B, E are enlargements of A, D, respectively. The scale bars indicate 100 μm in A, C, D, and F. Images are representative of the number (n) of the seedlings that were studied.

Supplemental Figure 3. Measurement of hormone content. (A) Macrophotograph of Stage I; (B) shows the corresponding hormone content. (C) Macrograph of a 10-week-old date palm seedling after germination. The purple arrowhead points to the structure protecting the seedlings. The white arrowhead indicates the shoot apical meristem. (D) Hormone contents in different tissues of date palm seedlings. The y-axis represents hormone concentration, the x-axis represents organ types. The bars represent the mean ± SD; n=4 biological replicates; statistical analysis was performed using one-way analysis of variance (ANOVA) and Tukey's post hoc test. Different letters denote significant differences ($P < 0.05$); NS, non-significant. Abbreviations: PET,

petiole; SAM, shoot apical meristem; R, root; GA, gibberellic acid; JA, jasmonic acid; SA, salicylic acid; ABA, abscisic acid. The scale bar is 2 cm.

Supplemental Figure 4. Conserved function of date palm *SHORTROOT* in *Arabidopsis thaliana*

(A, B) Longitudinal section of a 12-week-old root stained with Lugol. The oval in B surrounds the stem cell niche (SCN) and starch granules marking differentiated columella cells. (C) In situ hybridization in tissue sections from 7-month-old date palm plants using *PdSHR*. (D) Functional complementation of *PdSHR* in Arabidopsis. The graph shows the average root length measurements in WT (n=82), *shr* (n=11) and *AtpSHR:PdSHR* in *shr* (n=84). Error bars represent the ± standard errors.

827 Supplemental Table 1. Primers used in this study

PdSTM-F	GAATTATGTCGATCCTCAAGCTG
PdSTM-R	GGGAAAGGGATTGCCGAG
PdSHR-F	GACGACACGCCTCACCT
PdSHR-R	CACGTCCTCACTGAACGCC
PdSMB-F	GGGCAGCTCACCGTGCC
PdSMB-R	TCATGCATGATCCAGTC
PdHISTONEH4-F	ATAGCTCAAGTGAGATCATC
PdHISTONEH4-R	GAGAACAATGAGGCACTGCATTC
PdIAA2-F	CATCACCTCTACATCCTCCTTAG
PdIAA2-R	CTCTTGTATTACATGCTAATTTCTACAC
PdAINT-F	ATGGCTCCGAAGAACCCCGCACCT
PdAINT-R	CGGGGTCCGATACCGAGACG
PdSHRgenomic-F	GGGGACAAGTTTGTACAAAAAAGCAGGCTGTTCCTCTCC AAGTTGAAGCCTCCCTTAGCTCAATTCCG
PdSHRgenomic-R	GGGGACCACTTTGTACAAGAAAGCTGGGTTTAATAATAG CCGTCATGATGACAATATCTTGT

828

829

Supplemental Table 2. RNAseq reads per sample

Sample	Reads (2x150)	Gbases
Embryo Rep1	15,129,278	4.538
Embryo Rep2	18,626,253	5.587
Root Rep1	23,558,342	7.067
Root Rep2	16,838,937	5.051

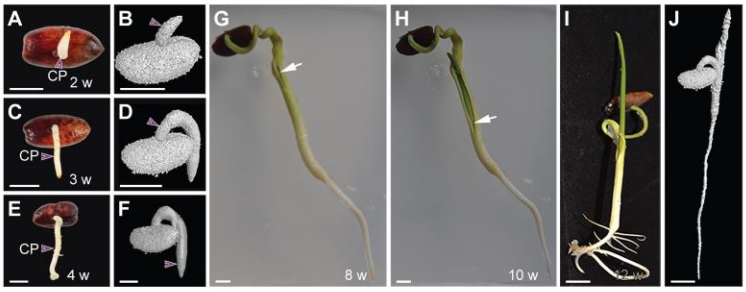

Figure 1. The germination process in date palms.
(A-F) 2-4 weeks after germination; (G) 8 weeks after germination, (H) 10 weeks after germination and (I-J) 12 weeks after germination. A, C, E and G-I are macrophotographs. B, D, F and J are images obtained from 3D X-ray computed tomography. The white arrows in G and H point to tissue apertures allowing leaves to emerge; purple arrowheads point to the cotyledonary petiole (CP). Abbreviations: w, weeks after germination. The scale bars are 1 cm. Images are representative of 40 seedlings.

833

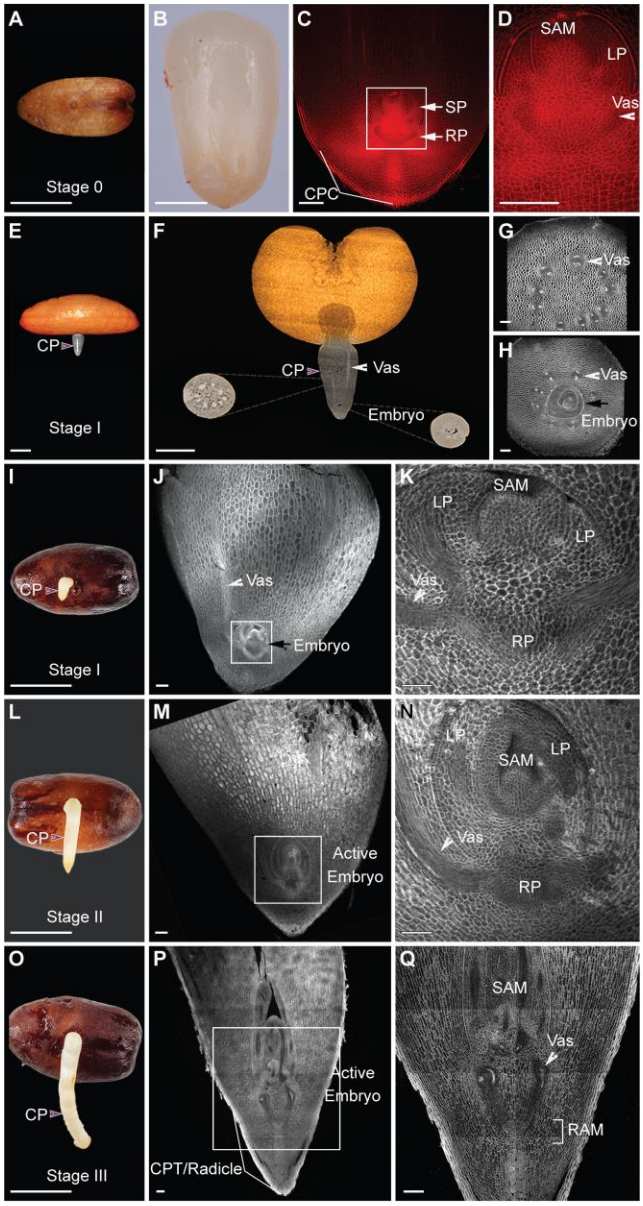

Figure 2. Growth dynamics during germination in date palms.

(A) Date palm seed containing the embryo. (B) Embryonic sac dissected from the seed (n= 20). (C, D) Longitudinal section of dissected embryo sac stained with modified pseudo-Schiff propidium iodide (mPS-PI) (n=20). The white arrows indicate root and shoot axes in C. (E, F) 3D image of germinated date palm at Stage I imaged with XμCT (n=3). (G,H) Confocal images of cotyledonary petiole sections taken at the same stage as F. The section in (G) at the upper part, which does not include the embryo; the section in (H) includes a transverse view of the embryo (n=15). (I-Q) Date palm growth at 1-4 weeks after germination (n=25). I, L, and O are macrophotographs; J, K, M, N, P, and Q are confocal images of longitudinal vibratome sections with the cell walls stained with SCRI Renaissance 2200 (n=10). White arrowheads point to the vasculature (Vas); purple arrowheads point to the cotyledonary petiole (CP). The black arrows in H and J indicate the embryo. Abbreviations: RP, root pole; SP, shoot pole; SAM, shoot apical meristem; LP, leaf primordia; RAM, root apical meristem; CPT, cotyledonary petiole tip. D, K, N, and Q are insets of C, J, M and P, respectively. The scale bars indicate: A, 1 cm; B, 0.5 cm; C and D, 100 μm; E, 5 mm; F, 2 mm; G, C and H, 100 μm; I, L, and O, 1 cm; G, M, and P, 100 μm; K, N and P, 50 μm. Images are representative of the total number (n) of seedlings that were studied.

834

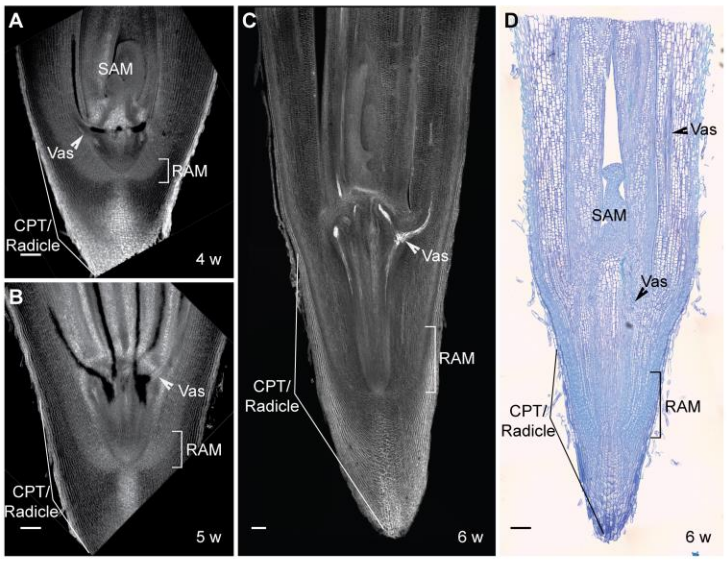

Figure 3. Encapsulated organogenesis in date palm.
(A-C) Confocal images of 4-6 weeks longitudinal sections of date palm stained with mPS-PI. (D) DIC images of the longitudinal plastic section stained with Toluidine blue O. Abbreviations: RAM, root apical meristem; SAM, shoot apical meristem; ESJ, root-shoot junction; Vas, vasculature; CPT, cotyledonary petiole tip; w, weeks after germination. Scale bars indicate 100 µm. Images are representative of 10 seedlings that were studied.

835

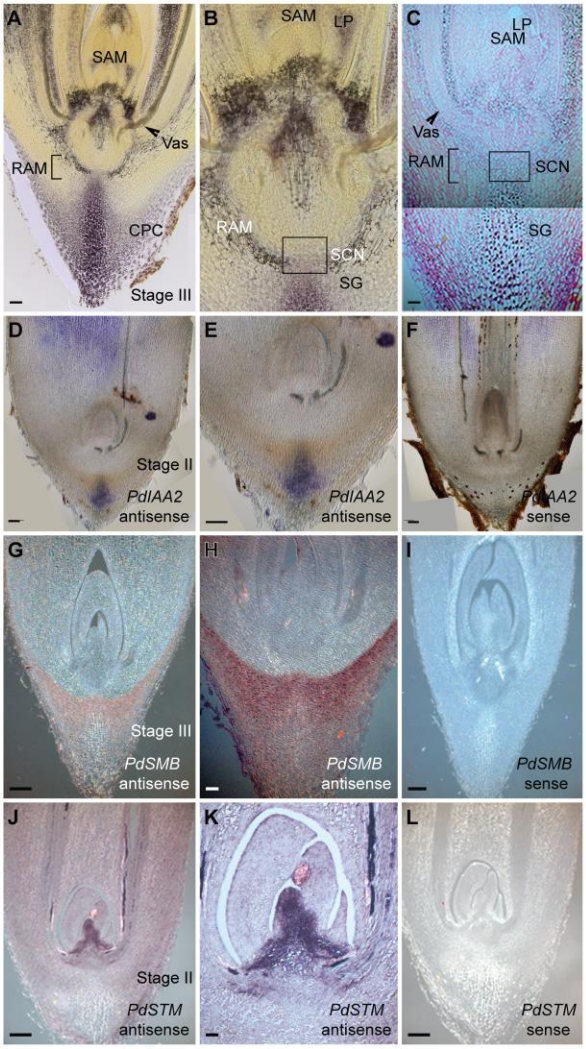

Figure 4. Characterization of root and shoot meristem in date palm.
(A-C) Accumulation of starch granules at the root tip. Light microscope images of vibratome sections stained with Lugol (A, B; n=8; brown color). Plastic longitudinal sections stained with ruthenium red (pink color) and Lugol (C; n=8). (D-F) Gene expression analysis with in situ hybridization using the date palm auxin response gene *IAA2* (*PdIAA2*); antisense probe (D, E; n=15; mRNA signal is shown in blue/purple); sense control (F; n=15). (G-I) Differentiated columella layers are marked with date palm *SOMBRERO* (*PdSMB*). The antisense probe (G, H; n=10; mRNA signal is shown in brown) is compared with the sense control for *PdSMB* (I; n=10). (J-L) The shoot meristem is marked with *SHOOT MERISTEMLESS* gene (*PdSTM*), the antisense probe (J, K; n=9; mRNA signal is shown in brown); sense control for *PdSTM* (L; n=9). E, H, K are zoomed in from D, G, J respectively. Abbreviations: SCN, stem cell niche; SG, starch granules; CPC, cotyledonary petiole cap; SAM, shoot apical meristem; LP, leaf primordia; RAM, root apical meristem. Scale bars indicate: A and C, 50 µm; D-F, 100 µm; G, I, J, and L, 200 µm; H, 100 µm; K, 50 µm. Images are representative of the total number (n) of seedlings that were studied.

836

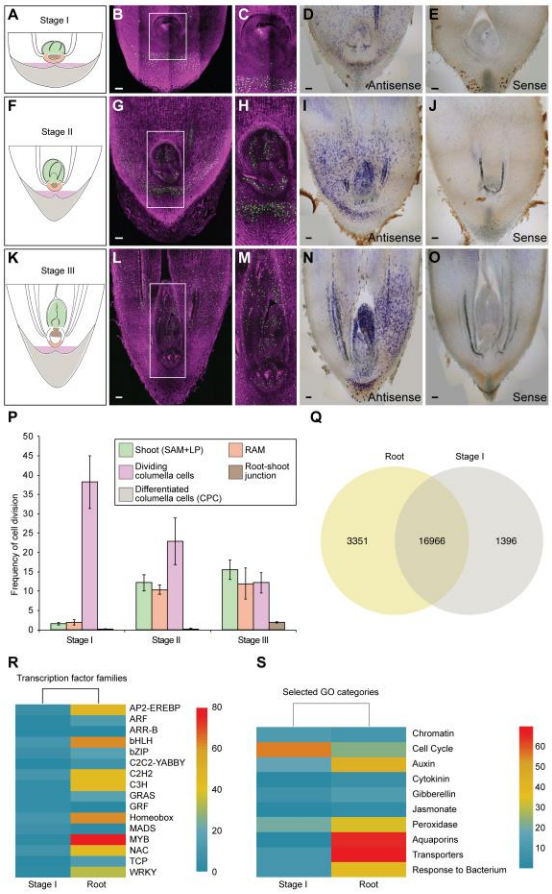

Figure 5. Postembryonic development correlates with an increase in cell division rates and activation of developmental genes.

(A, F, K) Cartoons representing the early developmental stages of date palms, Stage I (A-E), Stage II (F-J) and Stage III (K-O). (B, C, G, H, L, M). Confocal images of vibratome sections from the cotyledonary petiole showing dividing cells as captured by EdU staining (n= 35). Dividing EdU stained nuclei are shown in green; nuclei counterstained with Hoechst 33258 are shown in magenta. C, H and M are inset from B, G, and L, respectively. Scale bars indicate 100 µm. (D, E, I, J, N, O) In situ hybridization showing *PdHistone-H4* expression (n=20; signal is shown in blue/purple color). B-E, G-J, L-O are representative images of the total number (n) of seedlings that were studied. (P) Graph showing cell division rates in different zones and at different developmental stages of the seedlings. The x-axis represents developmental stages and the y-axis represents the measured frequency of cells incorporating EdU. Each column represents the average cell division frequency in a specific zone of the tip of the cotyledonary petiole. Error bars represent the ± standard errors. Numbers (n) of seedlings that were used: Stage I, n=14; Stage II, n=12; Stage III, n=6. Average nuclei counted (Hoechst) for the cell division frequency calculation per stage and per zone represented as follows. Shoot: RAM: dividing columella: root-shoot junction, 604: 210: 342: 97 (Stage I), 557:275:376:105 (Stage II) and 597, 494, 271, 107 (Stage III), respectively. Zones are indicated in colors in (A, F and K): Shoot (green); RAM (orange); dividing columella (pink); root-shoot junction (brown); cotyledonary petiole cap (CPC) (light brown). Measured zones are represented in P. (Q) Venn diagram showing overlapping and differentially expressed genes in Stage I and 12-week-old roots resulting from RNA-seq data. (R) Heat map representation of differentially expressed developmental genes. (S) Selected categories of enriched gene ontology (GO). Up-regulation is shown in red; downregulation is shown in blue.

837

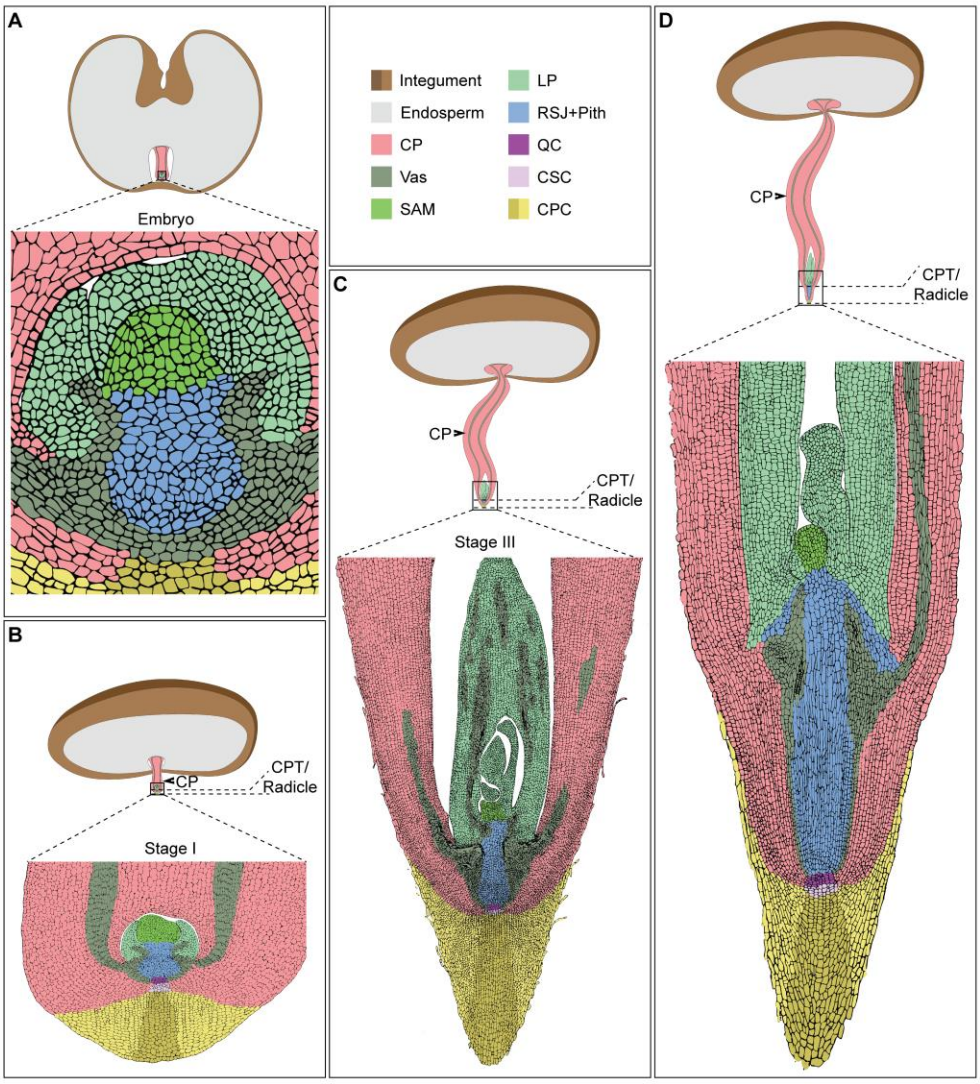

Figure 6. Schematic representations of date palm development from embryo to forming organs within the cotyledonary petiole. Representations are illustrations from longitudinal sections of real samples.
Black arrowheads points to the cotyledonary petiole (CP). Abbreviations: Vas; vasculature, LP; leaf primordia, RSJ; root-shoot junction, QC; quiescent center; CSC; columella stem cells; CPC, cotyledonary petiole cap.

838

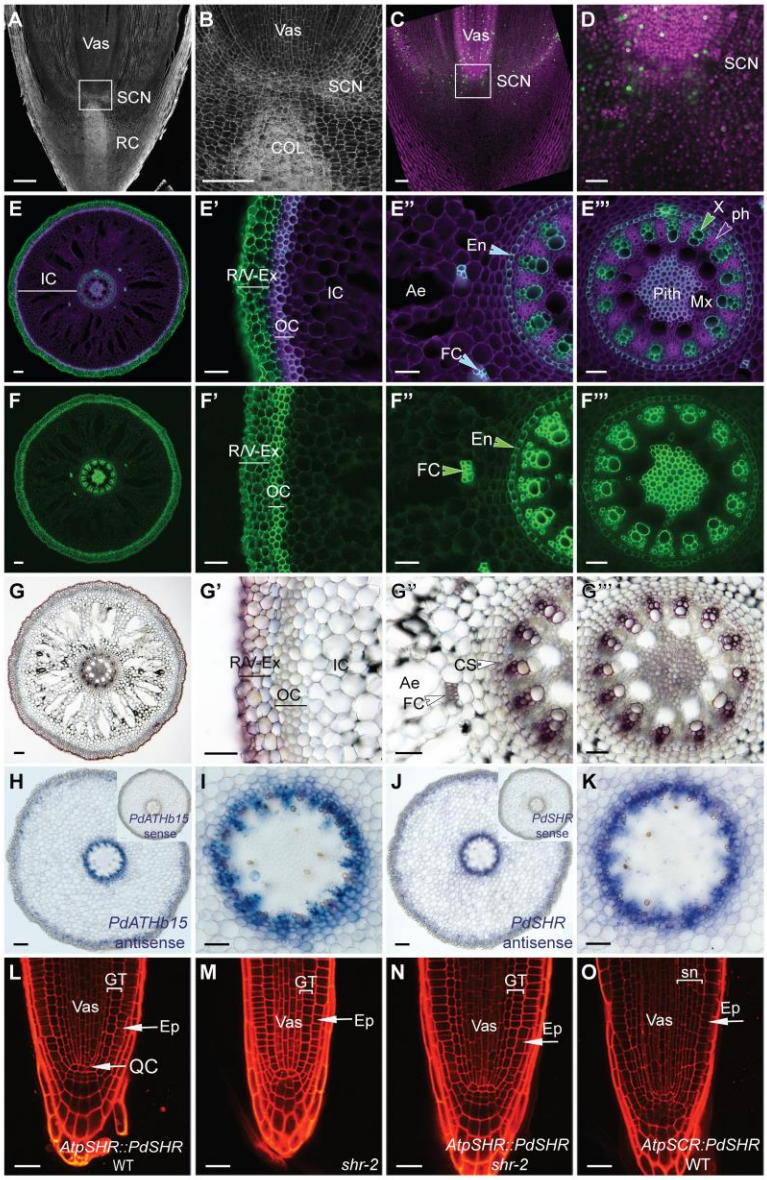

Figure 7. Date palm root anatomy.

(A, B) Confocal scanning images of longitudinal sections of roots obtained from 7 month old plants and stained with mPS-PI (n=3). (C, D) Dividing nuclei are stained with EdU (green) (n=5). Nuclei were counterstained with Hoechst (purple). (E-F''') Confocal image of a cross-section of a root stained with SCRI Renaissance 2200. Purple indicates cell wall staining; green is the auto-fluorescence marking lignin and suberin deposition within the roots (E-E'''). A berberine stained cross-section marks suberin in green (F-F'''). (G-G''') Lignin accumulation in a cross-section stained with Phluoglucocinol in dark brown. (H-K) RNA in situ hybridization in 12 week old roots. Signal blue/purple shows mRNA localization of vascular *PdATHB15* (H, I) and *PdSHR* (J, K) in date palm roots. Date palm SHR function is conserved in Arabidopsis. (L-O) Confocal images of a root stained with Propidium Iodide of *AtpSHR::PdSHR* in WT (L; n=6); *shr* mutant (M; n=6); *AtpSHR::PdSHR* in *shr* (N; n=8) and *AtpSCR::PdSHR* in WT (O; n=6). B, D, E'-E''', F'-F''', G'-G''' I and K show zoomed images from A, C, E, F, G, H and J, respectively. Abbreviations: SCN, stem cell niche; Col, columella; Vas, vasculature; R/V, rhizodermis/velamen; Ex, exodermis; OC, outer cortex; IC, inner cortex; En, endodermis; CS, Casparian strips; Mx, metaxylem; Ph; phloem; X, xylem; Ae, aerenchyma; FC, fiber cells; Ep, Epidermis; GT, Ground tissue: cortex and endodermis, Sn, supernumerary layers. The scale bars indicate 100 µm in A, C, E, F, G, H and J; 50 µm in B, D, E'-E''', F'-F''', G'-G''', I and K; 20 µm in L-O. Images are representative of the total number (n) of roots that were studied.

839

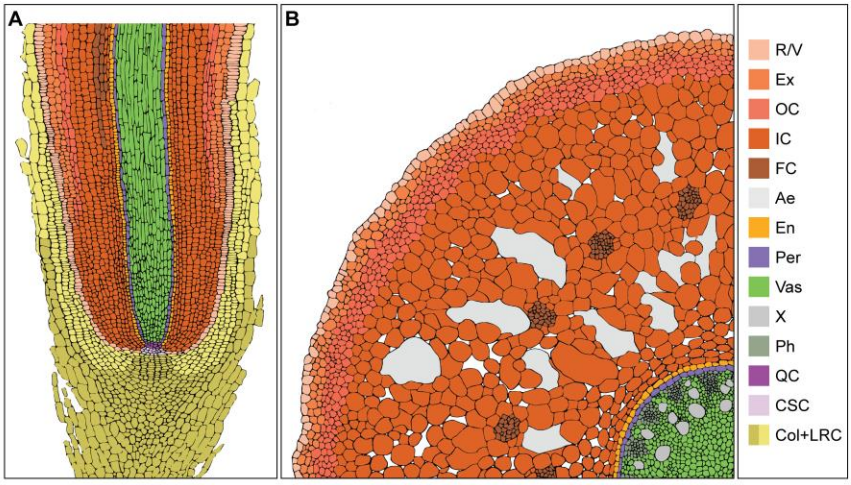

Figure 8. Schematic representation of the date palm root.
(A) Longitudinal section, (B) cross section. Colors represent distinct tissue types. Abbreviations: R/V: rhizodermis/velamen; Ex, exodermis; OC: outer cortex; IC, inner cortex; Ae, aerenchyma; FC, fiber cells; En, endodermis; Per, pericycle; Ph; phloem; X, xylem; Vas, vasculature; Col+LRC, columella and lateral root cap; CSC, columella stem cells; QC, quiescent center.

840

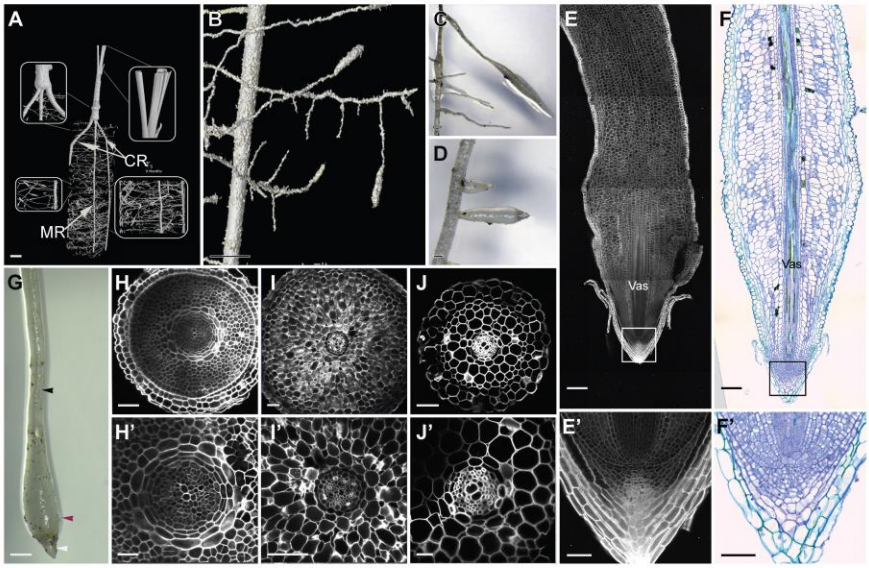

Figure 9. Characterization of date palm pneumatophores.
(A, B) X-ray micro-computed tomography images showing the root system architecture of the date palm: the primary root with secondary lateral horizontal growth and aerial roots with upward vertical growth. (B) is a zoomed image of A. (C, D, G) micrographs showing pneumatophores (n=10). (E, E') Longitudinal sections of date palm pneumatophores stained with mPS-PI (n=5). (F, F') DIC images of sections stained with Toluidine blue O (n=5). (H-J') Cross-sections of different zones within the pneumatophore (n=5); basal thin region (white arrowhead; H, H'), basal thick region (purple arrowhead; I, I') and apical thin region (black arrowhead; J, J'). E' F' H', I', and J' are enlargements of E, F, H, I, and J respectively. Abbreviations: MR, main root, CR, crown root. The scale bars indicate: A, 20 mm; B, 4.5 mm; C, D, G, 1 cm; E, F, 100 µm; H, I, J, E', F' 50µm; H', I', J' 25 µm. Images are representative of the total number (n) of roots that were studied.

841

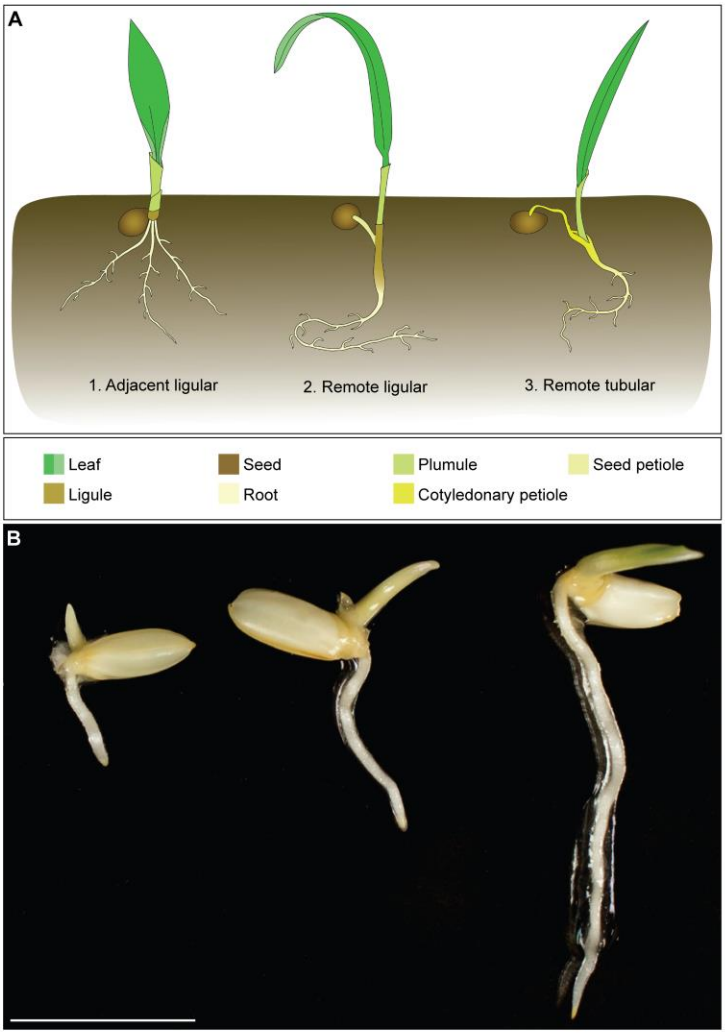

Supplementary Figure 1. Germination modes in palms and rice.
(A) Schematic representation of the different modes of germination in palms adapted from (Henderson, 2006). (B) Macrograph showing rice 1-, 2- and 3-days after germination (B; n=10). The scale bar in B is 1 cm.

842

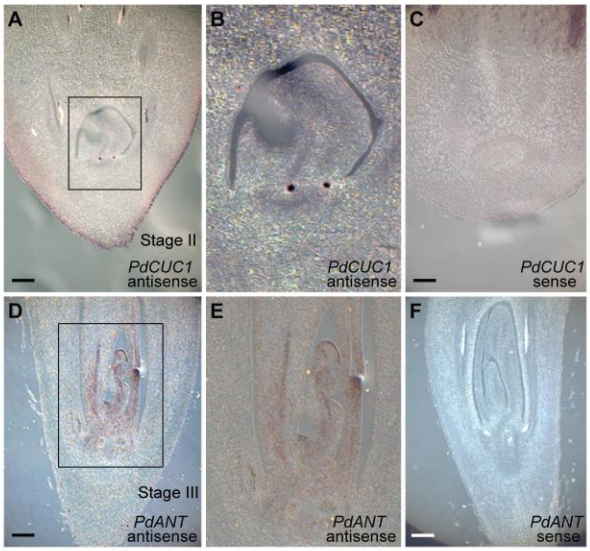

Supplementary Figure 2. Expression analysis of genes marking the shoot meristem and organ primordia.
In situ hybridization in a tissue section using gene delimiting organ boundaries *CUP-SHAPED COTYLEDON* (*PdCUC*) and primordial gene *AINTEGUMENTA* (*PdANT*). A, B, D, E are antisense probes (n=8), whereas C (n=5), F (n=7) are sense probes. B, E are enlargements of A, D, respectively. The scale bars indicate 100 µm in A, C, D, and F. Images are representative of the number (n) of the seedlings that were studied.

843

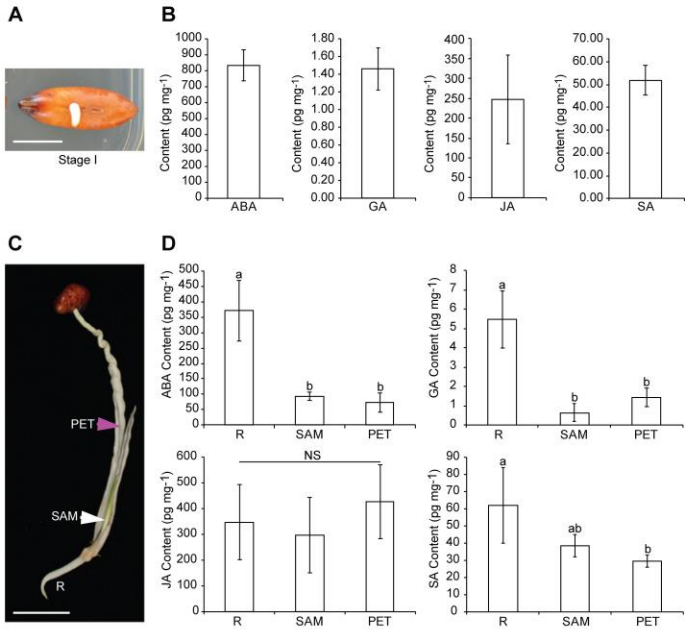

Supplementary Figure 3. Measurement of hormone content.
(A) Macrophotograph of Stage I; (B) shows the corresponding hormone content. (C) Macrograph of a 10-week-old date palm seedling after germination. The purple arrowhead points to the structure protecting the seedlings. The white arrowhead indicates the shoot apical meristem. (D) Hormone content in different tissues of date palm seedlings. The y-axis represents hormone concentration, the x-axis represents organ types. The bars represent the mean ± SD; n=4 biological replicates; statistical analysis was performed using one-way analysis of variance (ANOVA) and Tukey's post hoc test. Different letters denote significant differences ($P < 0.05$); NS, non-significant. Abbreviations: PET, petiole; SAM, shoot apical meristem; R, root; GA, Gibberellic acid; JA, Jasmonic acid; SA, Salicylic acid; ABA, abscisic acid. The scale bar is 2 cm.

844

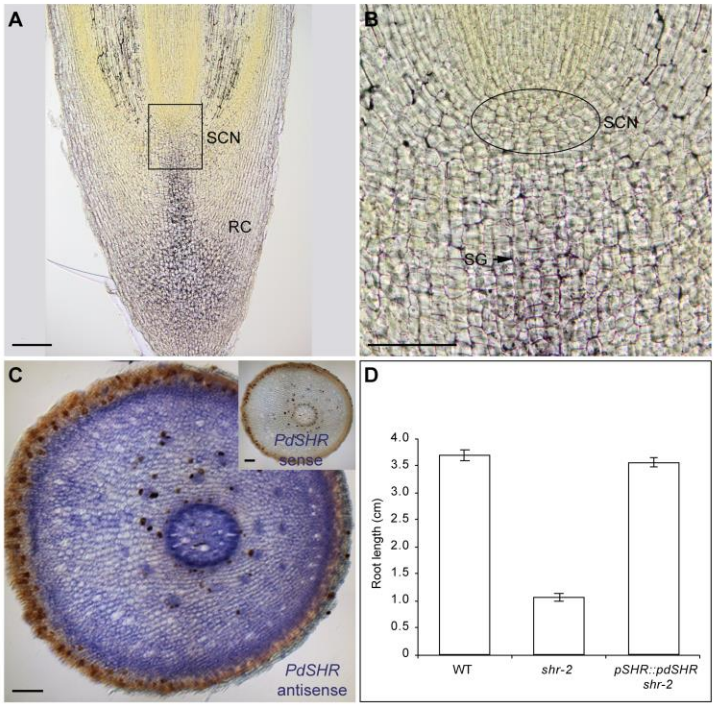

Supplementary Figure 4. (A, B) Longitudinal section of a 12 week old root stained with Lugol. The oval in B surrounds the stem cell niche (SCN) and starch granules marking differentiated columella cells. (C) In situ hybridization in tissue sections from 7 month old date palm plants using *PdSHR*. (D) Functional complementation of *PdSHR* in Arabidopsis. The Graph shows the average root length measurements in WT (n=82), *shr* (n=11) and *AtpSHR::PdSHR* in *shr* (n=84). Error bars represent the ± standard errors.

845